Impact of nuclear dissipation on the fission dynamics within the Langevin approach

Li-Le Liu,[1,*] Xi-Zhen Wu,[1,†] Yong-Jing Chen,[1] Cai-Wan Shen,[2] Zhi-Gang Ge,[1] and Zhu-Xia Li[1,‡]
[1]*China Nuclear Data Center, China Institute of Atomic Energy, Beijing 102413, China*
[2]*School of Science, Huzhou University, Huzhou 313000, China*

(Received 17 November 2021; accepted 4 March 2022; published 23 March 2022)

The impact of nuclear dissipation on the dynamics of nuclear fission at low excitation energy is studied with a three-dimensional Langevin approach in which the two-center shell model is adopted to describe the nuclear shape and the single-particle potential. With three types of formulas for the friction tensor, such as the wall formula, the wall-and-window formula with and without the term related to the mass asymmetry change, the fragment mass and the total kinetic energy (TKE) distributions in low-energy fission are calculated. The calculated fragment mass distributions are almost identical for both with the wall formula and with the wall-and-window model without the term related to the mass asymmetry change, and both the results are consistent with the evaluated mass yields and the calculated results with the GEF model. Our study found that the term related to the mass asymmetry change in the window formula leads to an unreasonable shift of the peak position of the mass distribution. The TKE values calculated with the wall model are slightly larger than those with the wall-and-window model due to the more compact configuration obtained with the pure wall model. Moreover, the influences of the strength of friction tensor on the fragment distribution, the scission configuration, and the fission time distribution are investigated. With the present model the fission fragment mass distributions of U, Np, Pu, and Am isotopes are well reproduced and the systematic dependence of the averaged TKE on the Coulomb parameter is also well reproduced.

DOI: 10.1103/PhysRevC.105.034614

I. INTRODUCTION

Nuclear fission involves a large-amplitude and strongly damping collective motion. The dynamical evolution of the fissioning nucleus is generally viewed as the motion of a Brownian particle in a heat bath, and the multidimensional Langevin approach has been adopted by many groups to study nuclear fission [1–14] and heavy-ion fusion reactions [15–18], based on the realistic potential energy surface, the deformation-dependent inertia tensor and friction tensor. Not only does the potential energy surface [19–22] dominate the optimal fission path and fission probability, but also nuclear dissipation has a crucial influence on the fission dynamics. Up to now, many progresses have been made in describing the dissipation mechanism [23–28] and investigating the influence of nuclear dissipation on the fission process and fission observables [1,4,6,29–39], mainly including the fission probability, the pre-scission multiplicity of neutrons, and the total kinetic energy (TKE) of fragments, etc. However, the effect of the strength of dissipation on the fission time and the scission configuration is still uncertain.

The microscopic linear response theory could be adopted to calculate the deformation and temperature dependent friction tensor [10,27,28], however, the method is much more difficult and time consuming. In the study of fission of a heavy nucleus, the energy dissipation during the dynamical process is usually described with the macroscopic one-body model [23,26,30] or the two-body model [24], and the difference between them comes from the mechanism of the exchange of energy between collective and internal degrees of freedom. The dissipation in the fission process at low excitation energy can be better described with the one-body model which involves the independent-particle model [4,30,35], and the two-body model is more applicable for the high-energy fission. In the framework of the one-body model, three main types of formulas were used to evaluate the friction tensor in the previous studies of low-energy fission: the wall formula [34,40,41], the wall-and-window formula with [10,12,13] and without the term of the rate of volume change (mass asymmetry) in the window formula [9,11]. However, knowledge of sensitivity of the fragment mass distribution and the TKE distribution to different types of friction tensor in low-energy fission is still lacking and needs further study.

In the present work, the influence of nuclear dissipation on fission dynamics at low excitation energy is studied using a three-dimensional Langevin approach, where the potential energy surface is obtained with the macroscopic-microscopic model based on the two-center shell model, and the friction tensor is calculated with the one-body wall formula and the wall-and-window formula, respectively. Based on the wall-and-window model, the effect of the term related to the volume change (the second term) in the window formula on the fission fragment mass and the TKE distribution is discussed. It is found that both the wall model for the

*liulile401@163.com
†lizwux9@ciae.ac.cn
‡lizwux@sina.com

friction tensor and the wall-and-window model without the second term in the window formula could better describe the fragment mass distribution of low-energy fission within the three-dimensional Langevin approach than that with the second term in the window formula which leads to an unreasonable shift of the peak position. Moreover, the influence of the strength of nuclear dissipation on the fission fragment mass distribution, the distribution of the TKE and the prescission collective kinetic energy and the Coulomb repulsion energy at the scission point, the scission configuration and the fission time distribution, etc., is investigated. Lastly, the fragment mass distributions in 14 MeV $n + {}^{232\text{–}239}$U, ${}^{233\text{–}240}$Np, ${}^{235\text{–}242}$Pu, ${}^{237\text{–}244}$Am fission are calculated and the systematic dependence of the averaged TKE on the Coulomb parameter is described, and most of the results agree well with the experimental data.

This paper is organized as follows. An introduction of the model is presented in Sec. II. The calculated results and discussions are shown in Sec. III. In Sec. IV, a summary of the present work and future prospects are presented.

II. METHODS

A. The Langevin approach

The dynamical process of nuclear fission can be viewed as an evolution of the nuclear shape from that of a single compound nucleus to the two receding fragments. In this work, the time evolution of the fissioning system is described within the stochastic approach based on the Langevin model, in which the slow collective motion is viewed as motion of a Brownian particle interacting stochastically with the inner nucleons, i.e., the "heat bath", under the assumption that the equilibration time of nucleons degrees of freedom is much shorter than the typical time scale of collective motion. The coupled Langevin equations describing the evolution of the collective coordinates $\{q_i\}$ and their conjugate momenta $\{p_i\}$ read

$$\begin{aligned}\frac{dq_i}{dt} &= (m^{-1})_{ij}p_j,\\ \frac{dp_i}{dt} &= -\frac{\partial V}{\partial q_i} - \frac{1}{2}\frac{\partial (m^{-1})_{jk}}{\partial q_i}p_j p_k - \gamma_{ij}(m^{-1})_{jk}p_k + g_{ij}\Gamma_j(t),\end{aligned} \tag{1}$$

where the summation convention for repeated indices is taken. $V(q)$ is the potential energy of deformation, $m_{ij}(q)$ and $\gamma_{ij}(q)$ are the shape-dependent inertia and friction tensor, respectively. The last term represents the random force, in which $\Gamma_j(t)$ is the normalized random force and obtained by using a Gaussian random number generator under the assumption of the white noise, and g_{ij} is the strength of the random force and determined from the fluctuation-dissipation theorem:

$$g_{ik}g_{jk} = \gamma_{ij}T^*, \tag{2}$$

where T^* is the effective temperature which takes into account the quantum effect at low excitation energy. The correlation between T^* and the nuclear temperature T [42] is

$$T^* = \frac{\hbar\varpi}{2}\coth\frac{\hbar\varpi}{2T}, \tag{3}$$

ϖ is the local frequency of the collective motion and we use the value $\hbar\varpi = 2$ MeV suggested in Ref. [43]. The temperature T is obtained with the Fermi gas model: $E_{\rm int} = aT^2$. The intrinsic excitation energy $E_{\rm int}$ is calculated at each step along the Langevin trajectory as follows:

$$E_{\rm int}(q) = E^* - \tfrac{1}{2}(m^{-1})_{ij}p_i p_j - V(q, T=0), \tag{4}$$

E^* is the total excitation energy of the compound nucleus, and for the fissioning systems populated by the 14 MeV neutron, the corresponding total excitation energies distribute around 20 MeV. In the present work, the particle evaporation along the Langevin trajectory is not taken into account, which will be further studied in future by coupling the statistical model into the Langevin calculation.

B. Potential energy

The potential energy surface of deformation for the fissioning system is one of the most fundamental ingredients of the Langevin approach, which dominates the optimal fission path and fission probability. In the present work, the potential energy of the fissioning nucleus is calculated within the framework of the macroscopic-microscopic model, and the nuclear shape is described based on the two-center shell model (TCSM) [44], which has an obvious advantage for describing the largely deformed nucleus and has been widely used in the study of nuclear fission [4,6,7,10,12,14] and heavy ion fusion reaction [45].

The potential energy within the macroscopic-microscopic model consists of macroscopic liquid-drop energy, and microscopic correction energy which origins from the contribution of quantum shell effect at zero temperature. The potential energy of deformation in nuclear fission is defined as the difference between the potential energy of a deformed nucleus and the corresponding spherical nucleus. The macroscopic potential energy is the sum of the deformation-dependent surface energy and the Coulomb energy calculated by using the finite range liquid drop model [46,47]. The microscopic energy contains the shell correction and the pairing correction, which are evaluated using the Strutinsky method [48] and the Bardeen-Cooper-Schrieffer method [49], respectively, based on the single-particle levels obtained from the TCSM in this work.

In order to describe the potential energy of the fissioning system at certain excitation energy, the temperature dependence is introduced for the microscopic correction energy as proposed in Ref. [50]:

$$V(q, T) = V_{\rm mac}(q) + V_{\rm mic}(q, T=0)\phi(T), \tag{5}$$

$$\phi(T) = \exp(-aT^2/E_d), \tag{6}$$

where the function of temperature dependence is expressed as an exponential suppression function in which the shell damping parameter is denoted by E_d and a represents the level density parameter of the compound nucleus. In this work, we use the standard Fermi-gas level density parameter, $a = A_{CN}/10$ MeV^{-1}, as that used in Ref. [34] which provides almost the same effect on the fission fragment mass distribution with the one given by the microscopic expression suggested by Ignatyuk [51]. Moreover, it is found that the

calculated mass distribution is insensitive to the parameter a in a reasonable range [14]. As for the shell damping parameter E_d, the value of 60 MeV is taken in the present calculation, and the calculated mass distribution for low-energy fission using Eq. (6) with $E_d = 60$ MeV is found to be similar to that with the expression proposed by Randrup and Möller [52]. It is assumed that the macroscopic energy is insensitive to the temperature at low excitation energy, and thus, the temperature dependence is not taken into account for the macroscopic energy. In addition, the angular momentum is small for nuclear fission induced by neutron at low energy, so it is neglected in the present work.

C. The inertia and friction tensor

In addition to the potential energy, the inertia tensor and friction tensor are also important ingredients of the dynamical model for describing the fission process, both of which are obtained within the framework of the macroscopic approach. In order to simplify the calculation, the nuclear shape is assumed to be axially symmetric along the z direction throughout the paper.

It is assumed that the nucleus is an incompressible and irrotational liquid drop. The Werner-Wheeler method [24] is adopted to calculate the inertia tensor, which is deformation-dependent and expressed as the following form:

$$m_{ij}(q) = \pi\rho_m \int_{z_{\min}}^{z_{\max}} \rho_s^2(z,q)\left(A_i A_j + \frac{1}{8}\rho_s^2(z,q)A_i' A_j'\right)dz, \quad (7)$$

$$A_i = \frac{1}{\rho_s^2(z,q)}\frac{\partial}{\partial q_i}\int_z^{z_{\max}} \rho_s^2(z',q)dz', \quad (8)$$

where $\rho(z,q)$ is the transverse extension of the nucleus at the position z along the symmetry axis, and $q = \{q_i\}$ represents the deformation parameter within the TCSM. ρ_m denotes the mass density of the fissioning nucleus and A_i' is the differentiation of A_i with respect to z.

The friction tensor is obtained with the one-body model, in which the mean free paths of nucleons are considered to be comparable to or larger than the size of the system, and the exchange of energy between collective and internal degrees of freedom arises from collisions of inner nucleons and a moving boundary of the system. Within the framework of the one-body model, the wall formula and the wall-and-window formula [23,26,30] are applied for the friction tensor in the present work.

Under the hypothesis of the continued randomization of the nucleon motions due to the sufficiently irregular motion of the system boundary, the wall friction tensor is obtained and written as [23]

$$\gamma_{ij}^{\text{wall}}(q) = \frac{1}{2}\pi\rho_m\overline{\upsilon}\int_{z_{\min}}^{z_{\max}} dz\frac{\partial\rho_s^2}{\partial q_i}\frac{\partial\rho_s^2}{\partial q_j}\left[\rho_s^2 + \frac{1}{4}\left(\frac{\partial\rho_s^2}{\partial z}\right)^2\right]^{-1/2}, \quad (9)$$

where $\overline{\upsilon}$ is the average velocity of inner nucleons and related to the Fermi velocity by $\overline{\upsilon} = \frac{3}{4}\upsilon_f$.

When the nucleus is highly deformed and thus the neck becomes obviously identified where the two prefragments are formed and divided by a window located at the position of the smallest neck radius, any nucleons passing through the window will damp the motion due to the momentum transferred between the two prefragments. For this case, the window dissipation needs to be taken into account and the pure wall dissipation should be modified as the wall dissipation applying for motions of the prefragment walls relative to their respective centers of mass. Thus, the corresponding friction tensor is expressed as

$$\gamma_{ij}^{W+W}(q) = \gamma_{ij}^{\text{wall2}}(q) + \gamma_{ij}^{\text{window}}(q), \quad (10)$$

$$\gamma_{ij}^{\text{wall2}}(q) = \frac{1}{2}\pi\rho_m\overline{\upsilon}\int_{z_{\min}}^{z_{\max}} dz\left(\frac{\partial\rho_s^2}{\partial q_i} + \frac{\partial\rho_s^2}{\partial z}\frac{\partial D_\nu}{\partial q_i}\right) \times\left(\frac{\partial\rho_s^2}{\partial q_j} + \frac{\partial\rho_s^2}{\partial z}\frac{\partial D_\nu}{\partial q_j}\right)\left[\rho_s^2 + \frac{1}{4}\left(\frac{\partial\rho_s^2}{\partial z}\right)^2\right]^{-\frac{1}{2}}, \quad (11)$$

$$\gamma_{ij}^{\text{window}}(q) = \frac{\rho_m\overline{\upsilon}}{2}\Delta\sigma\frac{\partial R_{12}}{\partial q_i}\frac{\partial R_{12}}{\partial q_j}, \quad (12)$$

where D_ν ($\nu = L$ for the left part and $\nu = R$ for the right part) is the position of the mass center of the prefragment relative to the mass center of the whole system. $\Delta\sigma$ is the area of the window between two parts. R_{12} denotes the distance between the centers of mass of two parts.

The expression of Eq. (12) is the window formula for the energy dissipation associated with the relative motion of the two parts for the dinuclear shape. In the study of the deep-inelastic nuclear reaction, it is found that the window formula of Eq. (12) is incomplete and the dissipation associated with a time rate of the change of the mass asymmetry degree of freedom should be included, and it is found that without this term in the window formula, the deep-inelastic scattering cannot be reproduced in the dynamical model [25,53]. The corresponding window formula with this additional term is

$$\gamma_{ij}^{\text{window}'}(q) = \frac{\rho_m\overline{\upsilon}}{2}\left(\Delta\sigma\frac{\partial R_{12}}{\partial q_i}\frac{\partial R_{12}}{\partial q_j} + \frac{32}{9}\frac{1}{\Delta\sigma}\frac{\partial V_R}{\partial q_i}\frac{\partial V_R}{\partial q_j}\right), \quad (13)$$

where V_R is the volume of the right part of the window. For the three-dimensional TCSM, only the collective coordinate mass asymmetry η is relevant to the second term in Eq. (13) with $\frac{\partial V_R}{\partial\eta} = \frac{1}{2}V_{CN}$ and it provides only nonzero component $\gamma_{\eta\eta}^{\text{window}}$ to the second term of the right-hand side of Eq. (13). As this term directly affects the motion of the collective coordinate mass asymmetry, it may cause a shift of the fragment mass distribution in low-energy nuclear fission, while how large it influences the mass distribution is not known. In this work, Eqs. (12) and (13) are adopted for the window friction tensor, respectively, and thus, the influences of the second term in Eq. (13) on the fragment mass distribution and the TKE distribution can be investigated. In this work we focus on the influence of the second term in Eq. (13) on the U isotopes fission induced by neutron at 14 MeV.

During the whole fission process in which the nucleus evolves continuously from the mononuclear shape to dinuclear shape, a smooth transition between the pure wall friction and the wall-and-window friction suggested by Nix and Sierk

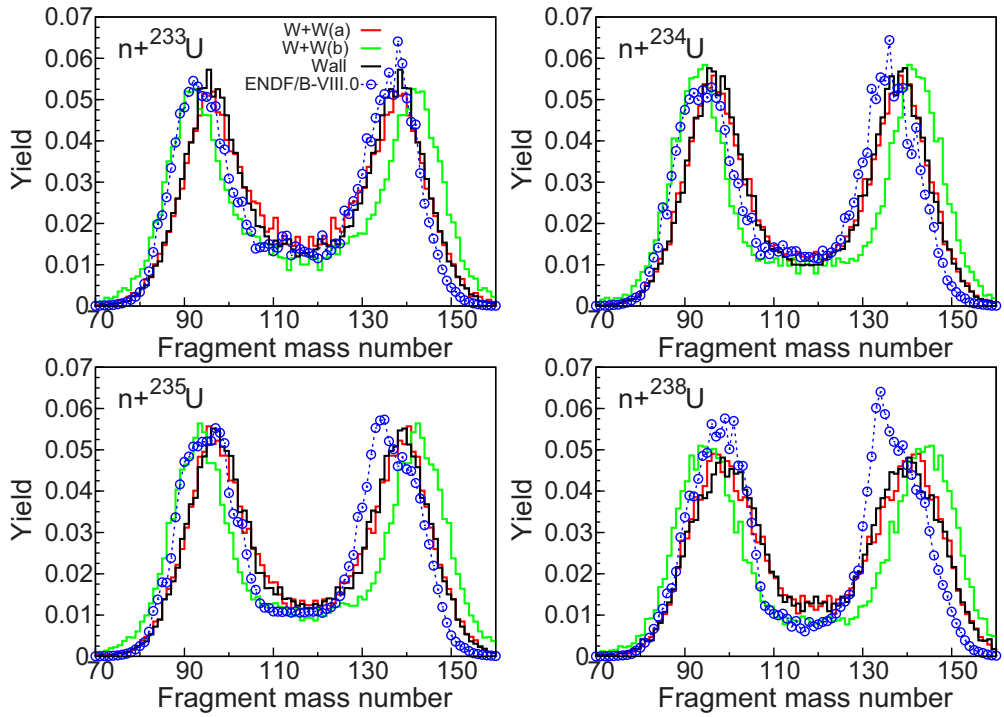

FIG. 1. The calculated fragment mass distribution in 14 MeV $n + {}^{233,234,235,238}\mathrm{U}$ fission in which the friction tensor is calculated with the wall-and-window formula where the window friction tensor is obtained using Eqs. (12) [W+W(a)] and (13) [W+W(b)], respectively, and the wall formula (black curve), compared with the evaluated data from ENDF/B-VIII.0 [55] (blue circle).

[54] is used and expressed in the following:

$$\gamma_{ij} = \tau\left(\gamma_{ij}^{W+W}\right) + (1-\tau)\gamma_{ij}^{\mathrm{wall}}, \tag{14}$$

$$\tau = \cos^2\left(\frac{\pi}{2}\frac{r_N^2}{b^2}\right), b = \min(b_1, b_2), \tag{15}$$

where r_N is the neck radius, and b denotes the lesser of the transverse semiaxis of the two prefragments.

III. CALCULATED RESULTS

In this work, the Langevin calculation is performed in the three-dimensional deformation space, and the corresponding collective coordinates $\{q_i\}$ are $\{Z_0/R_0, \delta, \eta\}$ within the two-center shell model parametrization [44], in which Z_0/R_0 is the elongation with the Z_0/R_0 being the distance between centers of prefragments normalized by the radius of the corresponding spherical nucleus and η is the mass asymmetry, and δ denotes the deformation of fragments. It is assumed that the semiellipsoid ends of the two fragments have the same deformations, i.e., $\delta_1 = \delta_2 = \delta$, which does not mean that the two fragments divided by the plane at $z = 0$ (neck position) have the same deformation. In addition, the neck parameter ϵ is fixed at 0.35 which is recommended in Ref. [27] for the fission process. During the calculation of Langevin trajectory, the potential energy, inertia tensor, and friction tensor at each step are obtained on the prepared meshes to save the computation time. The mesh values $\{Z_0/R_0, \delta, \eta\}$ are taken to be

$$Z_0/R_0 = -0.32(0.1)4.02, \quad \delta = -0.45(0.03)0.81,$$
$$\eta = -0.62(0.04)0.62.$$

The initial condition is set to be around the first saddle point $\{Z_0/R_0 = 0.5, \delta = 0.2, \eta = 0.0\}$ on the potential energy surface, and the scission point is determined by a fixed neck radius to be 0.5 fm. The number of the Langevin trajectories reaches at least 2.5×10^5 per fissioning system, which guarantees enough statistics for the calculated results.

A. The calculated fragment distributions with different types of friction tensor

The dissipation plays an important role in the dynamical process of nuclear fission. In this work, the influences of the dissipation on the fission fragment mass and TKE distribution are investigated by adopting three types of formulas for the friction tensor in the Langevin calculation, which are the wall formula [Eq. (9)], and the wall-and-window formula in which the window friction tensor is calculated with [Eq. (13)] and without the term representing the time rate of right fragment mass change [Eq. (12)], respectively. Figure 1 shows the calculated fragment mass distributions using different types of friction tensor for $^{233,234,235,238}\mathrm{U}$ fission induced by a neutron at 14 MeV, along with the evaluated data from ENDF/B-VIII.0 [55], where W+W(a) and W+W(b) denote the wall-and-window model with the window friction tensor obtained from Eqs. (12) and (13), respectively. It can be seen that the calculated fragment mass distributions are almost identical for both of the peak width and peak position when the friction tensor is calculated with the wall model and the W+W(a) model, respectively, and the results are overall consistent with the evaluated data. It means that the

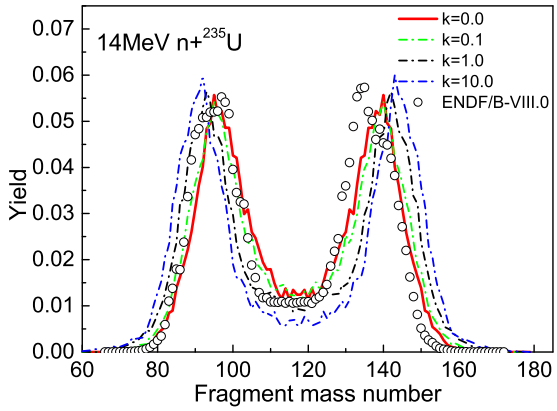

FIG. 2. The calculated fragment mass distribution in 14 MeV $n + {}^{235}\mathrm{U}$ fission with the second term (i.e., the rate of volume change of right fragment) of the window formula [Eq. (13)] multiplied by a factor of $k = 0.0$, 0.1, 1.0, 10.0, respectively, along with the evaluated data from ENDF/B-VIII.0.

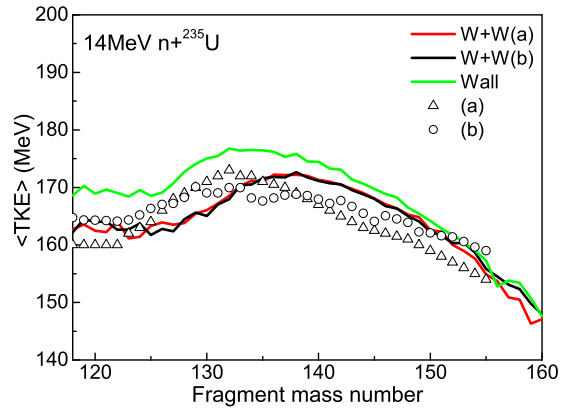

FIG. 3. The calculated TKE as a function of the heavy fragment mass in 14 MeV $n + {}^{235}\mathrm{U}$ fission in which the friction tensor is calculated with the wall-and-window formula where the window friction tensor is obtained using Eqs. (12) [W+W(a)] and (13) [W+W(b)], respectively, and the wall formula (green curve), along with the experimental data. The experimental data are taken from (a) [56] and (b) [57], respectively.

fission fragment mass distribution in the low-energy fission is insensitive to the energy dissipation of relative motion of two prefragments in the window formula, and the simple wall formula could reproduce the experimental data of the fragment mass distribution in the low-energy nuclear fission, which agrees with Refs. [23,34] and our previous work [40]. It should be noted that the present results are that of the primary fragments, so the slight deviation of the results of the wall model and the W+W(a) model from the evaluated data is reasonable, which should be improved by coupling the neutron evaporation model into the Langevin calculation.

However, when the additional term donating the time rate of mass change of the right fragment is introduced into the window formula [W+W(b) shown in Fig. 1], both the heavy and light fragment mass distributions for 14 MeV $n + {}^{233,234,235,238}\mathrm{U}$ fission shift towards two sides several mass units compared to the results from the wall model and the W+W(a) model, and the deviation from the evaluated data becomes quite large, which shows that this additional term in the window formula, i.e., the second term in Eq. (13), leads to the deviation of the peak position of the fission fragment mass distribution. In order to further study the influence of the additional term on the fission fragment mass distribution, the calculated results obtained by multiplying the additional term by a factor with different values are compared and shown in Fig. 2. One can see that the heavy fragment mass distribution shifts to the right side more mass units with the factor k becoming larger, and without this term ($k = 0.0$) the corresponding calculation result is more consistent with the evaluated data. It is well known that the additional term plays an important role in the deep-inelastic nuclear reaction, and without it the final asymmetries calculated with the dynamical model would most likely be zero [25,53]. Nevertheless, in the description of the low-energy nuclear fission, the additional term causes a shift leading to a deviation of the mass distribution of heavy fragments from that determined by the fission potential energy in which the shell correction plays essential roles. We find that this unreasonable shift of the peak position of the mass distribution for heavy fragments appears in the low energy fission of actinides within the TCSM approach. The effect of this term on the mass symmetric fission, such as the fission of Th and nuclides lighter than Th, as well as the superheavy nuclei, will be investigated in future work. As for the large discrepancy of the peak position in $n + {}^{238}\mathrm{U}$ shown in Fig. 1 for all three types of friction tensor, it is probably due to the strong shell correction of $^{132}\mathrm{Sn}$ as the N/Z ratio in $n + {}^{238}\mathrm{U}$ becomes closer to that of $^{132}\mathrm{Sn}$.

The TKE of fission fragments is another important observable which is quite sensitive to the dissipation. The dominant origin of the TKE is the Coulomb repulsion energy of fragments, which is approximately treated as that between two charged point particles located at the centers of mass of two fragments, and the other origin of the TKE is the prescission kinetic energy, which is defined as the collective kinetic energy at the scission point. With the above three types of formulas for the friction tensor, the TKE distribution in 14 MeV $n + {}^{235}\mathrm{U}$ fission is calculated and shown in Fig. 3. One can see that there is no significant difference between the calculated TKE distribution with W+W(a) and that with W+W(b), which indicates that the term representing the time rate of the fragment mass change has almost no influence on the TKE of fission fragments, and it implies that the influence of the additional term in W+W(b) on the shapes and the distance between centers of mass of two fragments is negligible, which is understandable as this term mainly affects the collective motion of mass asymmetry. However, the TKE values obtained from the wall model are slightly higher than that with the wall-and-window model, which is because of the fragment separation being strongly damped within the pure wall model leading to a more compact configuration [30].

In Fig. 3, we also show the comparison of the calculated TKE and the experimental data. It can be seen that the calculated results using the wall model are certainly slightly higher than the experimental data throughout the whole area, and the

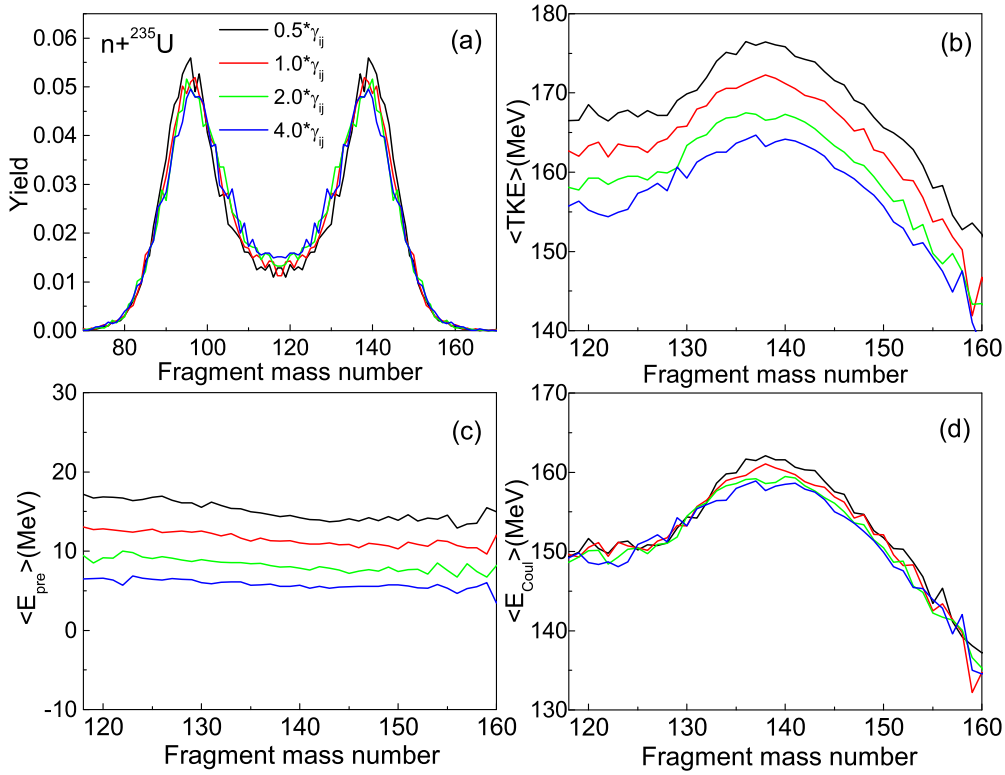

FIG. 4. The calculated mass distribution (a) and the TKE distribution of fragments (b) in 14 MeV $n + {}^{235}\mathrm{U}$ fission with the friction tensor multiplied by a factor of 0.5, 1.0, 2.0, 4.0, respectively. The corresponding collective kinetic energy (c) and the Coulomb energy at the scission point as a function of heavy fragment mass number (d) for each friction tensor. The friction tensor is calculated with the W+W(a).

results within the wall-and-window model agree well with the experimental data around the symmetric region, however, the corresponding calculated results are several MeV lower when the heavy fragment mass number A_H is around 130, and are several MeV higher when A_H is around 140. The deviation of the calculation results of TKE distribution from the experimental data may indicate that the shell correction of fragments around ^{132}Sn should be treated more rigorously, and thus, the shape of fragments around ^{132}Sn will be closer to spherical shape with little octupole deformation. To introduce different shapes of two ends of the fissioning nucleus (four-dimensional Langevin) may improve the TKE distribution around ^{132}Sn to a certain extent. From the above investigation of the influence of different forms of friction tensor on the mass and TKE distribution, it seems to us that the W+W(a) provides a better description of both observables, therefore, in the following calculations, the W+W(a) will be adopted.

B. The influence of the strength of friction tensor on the fragment distribution and the scission configuration

In this section, we investigate the influence of the strength of friction tensor on the fragment mass distribution, the TKE distribution and the scission configuration, taking the case of 14 MeV $n + {}^{235}\mathrm{U}$ fission as an example. The top panel of Fig. 4 shows the calculated fragment mass and TKE distribution with the friction tensor multiplied by a factor of 0.5, 1.0, 2.0, 4.0, respectively. It can be found that the mass distributions of fragments calculated with different friction strengths are roughly similar as they are mainly determined by potential energy surface for low-energy fission, which in some sense indicates the rationality and validity of the statistical scission-point models [58–61] in which the properties of fission fragment distributions can be determined from the potential energy of the fissioning system at the scission point, though mass distributions at the peak region are slightly suppressed and those at the symmetric region are enhanced slightly with the increase of friction strength. The TKE distribution is obviously affected by the strength of friction, and with the increase of dissipation the TKE decreases. The corresponding prescission kinetic energy and the Coulomb repulsion energy at the scission point are shown in Figs. 4(c) and 4(d), respectively. One can see that with the increase of the strength of friction, the prescission kinetic energy decreases with a relatively larger change, and the Coulomb repulsion energy is relatively less changed. It means that the decrease of the prescission kinetic energy contributes the large part and that of the Coulomb energy contributes to the small part of the decrease of TKE. The decrease of the pre-scission kinetic energy results from the slower evolution of the fissioning nucleus. While, the less decrease of the Coulomb repulsion energy indicates a nonobvious change of the elongation of the fissioning nucleus at the scission point with an increase in the strength of friction.

The scission configuration and the fission time obtained with the friction tensor multiplied by a factor of 0.5, 1.0, 2.0, 4.0 are shown in Fig. 5. The top panel of Fig. 5 shows the distributions of the nuclear elongation Z_0/R_0 and the

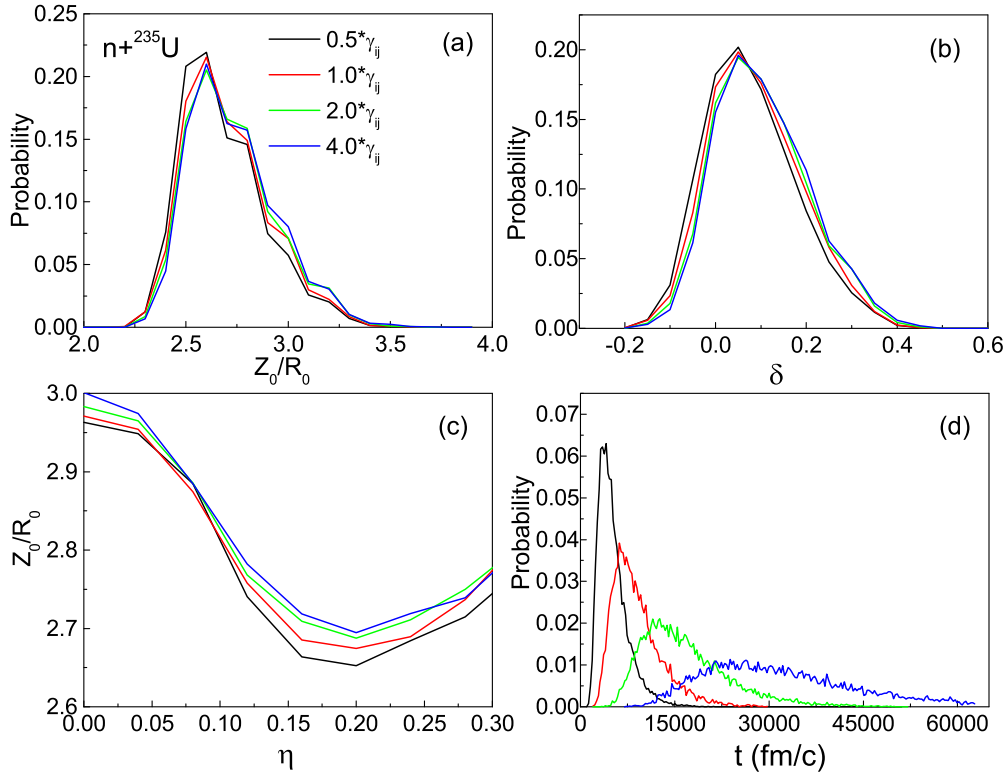

FIG. 5. The calculated distribution of the elongation parameter (a) and the deformation parameter δ at the scission point (b) in 14 MeV $n + {}^{235}$U fission with the friction tensor multiplied by a factor of 0.5, 1.0, 2.0, 4.0, respectively. The correlation between the averaged elongation and the mass asymmetry at the scission point (c), the distribution of the evolution time of fission events (starting from the first saddle point to the scission point) (d) for each friction tensor.

deformation δ at the scission point, both of which are the Gaussian-like distribution. One can see that with the increase of the strength of friction, the distribution of the elongation and that of the deformation shift slightly towards the right

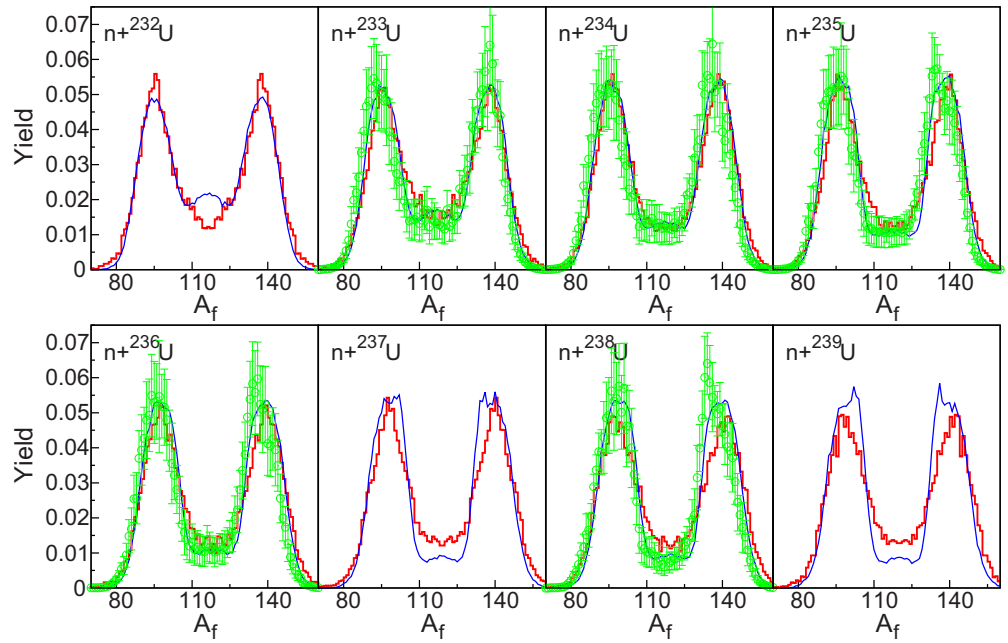

FIG. 6. The calculated fragment mass distribution in 14 MeV $n + {}^{232\text{–}239}$U fission (red curve), compared with the primary fragment mass distribution calculated with the GEF model (blue curve) and the evaluated data from ENDF/B-VIII.0 (green circle).

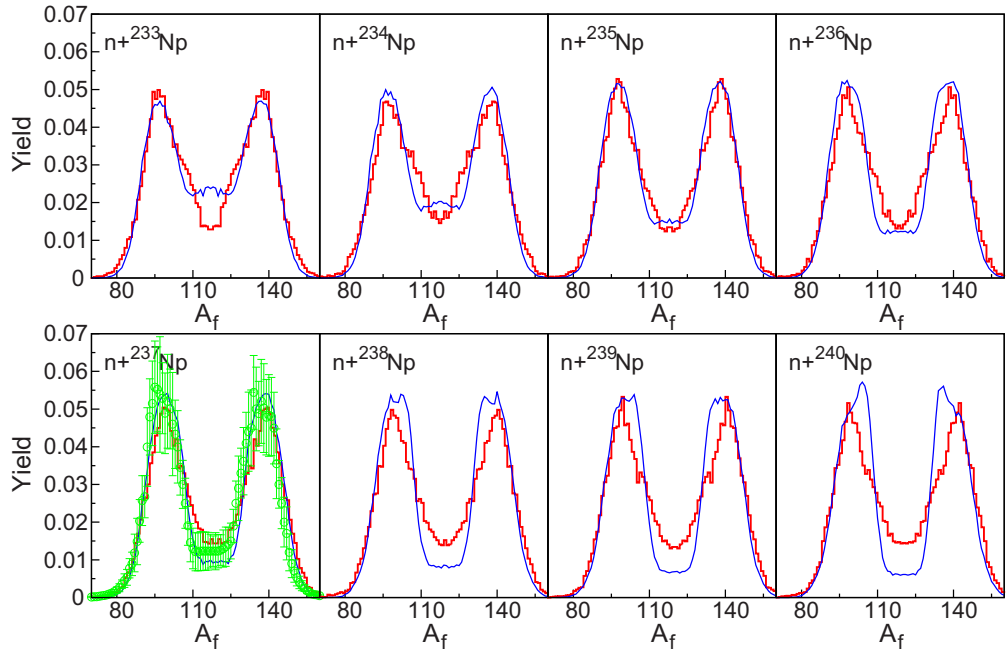

FIG. 7. The calculated fragment mass distribution in 14 MeV $n + {}^{233\text{–}240}$Np fission (red curve), compared with the primary fragment mass distribution calculated with the GEF model (blue curve) and the evaluated data from ENDF/B-VIII.0 (green circle).

side, which shows that the corresponding shape of the fissioning nucleus becomes slightly more elongated with the increase of dissipation, though the influence of the strength of friction on the nuclear shape is quite limited. On the whole, the most probable elongation parameter Z_0 and deformation parameter δ are around 2.6 R_0 and 0.05, respectively. In Fig. 5(c), we also show the correlation between the nuclear elongation Z_0 and the mass asymmetry η at the scission point for different strengths of friction tensor. The figure shows that the largest elongation is around the symmetric fission region, and the minimum is around $\eta \approx 0.175$ for all cases with different strengths of friction, which is in correspondence with the behavior of the TKE distribution shown in Fig. 4(b). With the increase of dissipation, the elongation increases obviously

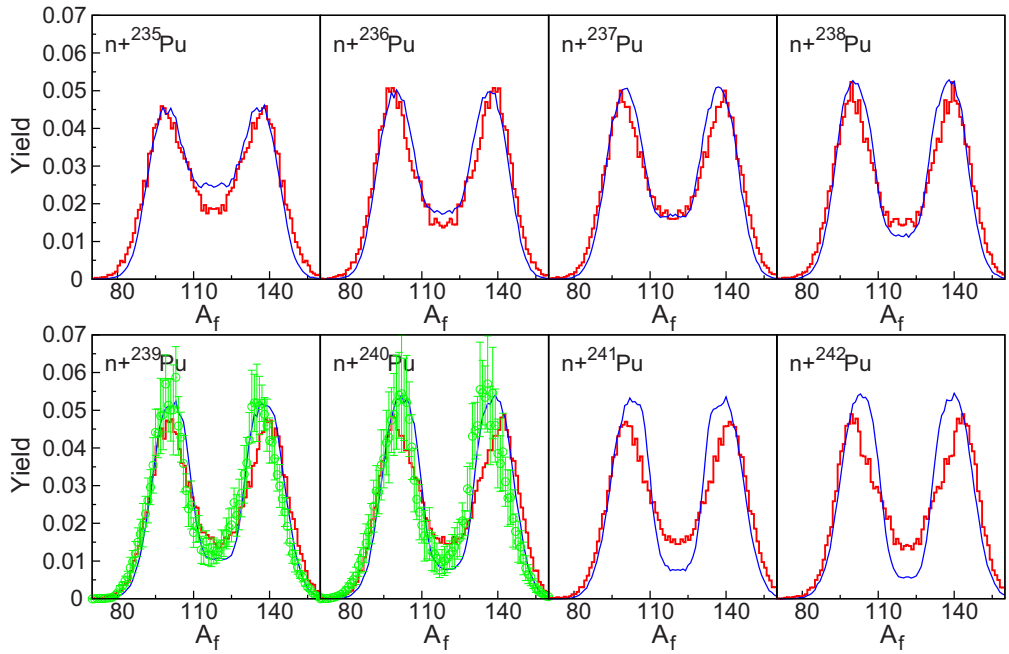

FIG. 8. The calculated fragment mass distribution in 14 MeV $n + {}^{235\text{–}242}$Pu fission (red curve), compared with the primary fragment mass distribution calculated with the GEF model (blue curve) and the evaluated data from ENDF/B-VIII.0 (green circle).

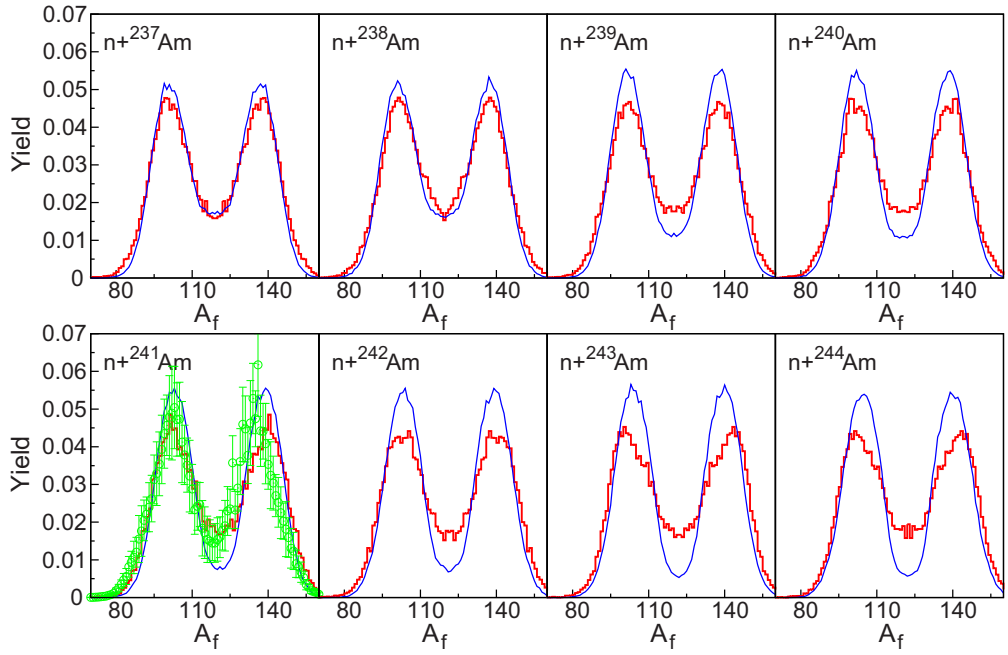

FIG. 9. The calculated fragment mass distribution in 14 MeV $n + {}^{237\text{–}244}$Am fission (red curve), compared with the primary fragment mass distribution calculated with the GEF model (blue curve) and the evaluated data from ENDF/B-VIII.0 (green circle).

around the valley region of asymmetric fission corresponding to the strong shell effect, and the maximum difference of elongation is about 0.05 R_0 when the factor of friction strength differs from 0.5 to 4.0. The influence of the strength of friction on the fission time distribution is also investigated and shown in Fig. 5(d). In the present work, the fission time is defined by the time spent for a Langevin trajectory from the first saddle point to the scission point. It can be seen that with the increase of the strength of friction, the fission time increases and its distribution width becomes wider. Moreover, the most probable fission time is proportional to the strength of friction. From the study of scission configuration and fission time we can conclude that with the increase of dissipation the fissioning system experiences a longer time to reach the scission point accompanying an increase of the dissipation of collective energy to internal excitation, leading to the mass distribution with an increase of symmetry fission and decrease of asymmetric fission as shown in Fig. 4(a). And simultaneously, the scission configuration becomes more elongated which is more obvious at the symmetric fission region and the peak region of asymmetric fission, especially the later one which slightly reduces the TKE energy around asymmetric fission region as shown in Fig. 4(d).

C. The calculated fragment mass distribution and the TKE for the fission of U, Np, Pu, and Am isotopes

The present model is extended to calculate the fission fragment mass distribution and the TKE for U, Np, Pu, and Am isotopes. Figures 6–9 show the calculated fragment mass distributions in 14 MeV $n + {}^{232\text{–}239}$U, ${}^{233\text{–}240}$Np, ${}^{235\text{–}242}$Pu, ${}^{237\text{–}244}$Am fission, compared with the evaluated data from ENDF/B-VIII.0 and the calculated preneutron mass yields with the GEF model [62]. It can be seen that most of the calculated results agree well with the evaluated data and the GEF calculated results, which verifies the predictive power of the present model. However, there is a trend that the deviation of the mass distribution from the evaluated data or GEF results increases with the increase of the ratio of N/Z for all the cases studied, which implies that the treatment of the shell correction around the closed shell $Z = 50, N = 82$ should be further improved in the calculation of potential energy.

The systematic dependence of the averaged TKE on the Coulomb parameter $Z^2/A^{1/3}$ of the fissioning systems from Pa

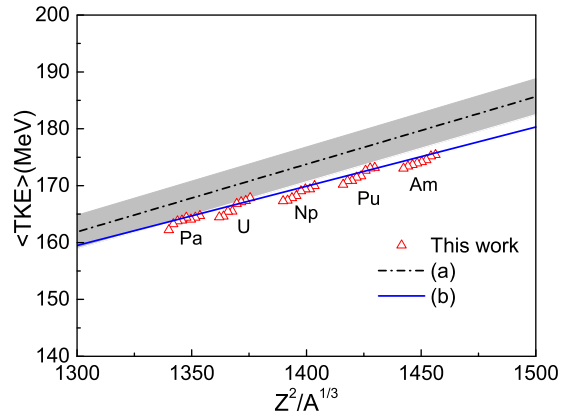

FIG. 10. The calculated systematic dependence of the averaged TKE on the Coulomb parameter $Z^2/A^{1/3}$ of the fissioning systems. The black dash-dotted line (a) and its shaded area show the Viola systematics [63]: $< E_k >= (0.1189 \pm 0.0011)Z^2/A^{1/3} + (7.3 \pm 1.5)$ MeV. The blue line (b) shows the systematics [64]: $< E_k >= 0.104Z^2/A^{1/3} + 24.3$ MeV.

to Am isotopes is also calculated and shown in Fig. 10, along with the calculated results with the systematic method [63,64]. The linear dependence of the averaged TKE on the Coulomb parameter is reproduced well, and the calculated results are overall consistent the systematics proposed by Itkis in 1998 [64], but lower than the Viola systematics [63]. Further work is needed for improving the mass distribution and the TKE of fission fragments. One is to increase the dimension of the Langevin equation. Another important aspect is to make a more exact treatment of the shell correction in the potential energy calculations.

IV. SUMMARY

In this work, the effect of the dissipation on the dynamics of nuclear fission at low excitation energy is studied with a three-dimensional Langevin approach. We first investigate the influence of the dissipation on the fission fragment mass distribution and the TKE distribution with three types of friction tensor in the Langevin calculation, i.e., the wall formula and the wall-and-window formula with [W+W(b)] and without the term representing the time rate of fragment mass asymmetry change [W+W(a)], respectively. The calculated fragment mass distributions with the wall formula and the W+W(a) are well consistent with the evaluated data from ENDF/B-VIII.0 and the results calculated with the GEF model, which indicates that the fragment mass distribution in low-energy fission is not very sensitive to the energy dissipation of relative motion of two prefragments in the window formula. The calculation with the W+W(b) for the friction tensor results in an unreasonable shift of the peak position of the heavy fragment mass distribution compared to the evaluated data. In addition, the calculated TKE distributions with the three types of formulas for the friction tensor show that the calculation with the W+W(a) is almost identical to that with the W+W(b), which means that the additional term related to the fragment mass asymmetry change has a slight effect on the TKE of fission fragments, and the TKE values with the wall model are overall larger because the fragment separation is strongly damped with the pure wall model leading to a more compact configuration. Therefore, the wall-and-window model without the term denoting the time rate of the fragment mass asymmetry change [W+W(a)] is adopted in the present work in order to describe both the fission fragment mass distribution and the TKE distribution.

Furthermore, the influences of the strength of friction tensor on the fission fragment mass distribution, the TKE distribution, and the scission configuration are investigated. The fragment mass distribution is insensitive to the friction strength, which in some sense justifies the fact that the statistical scission-point models describe the experimental data well, except at the symmetric fission region and the peak region of the asymmetric fission region where a slight influence is shown. However, the TKE of fragments becomes lower with the increase of dissipation. In addition, the elongation Z_0 and the deformation δ increase slightly with the increase of dissipation, which means that the corresponding shape of the fissioning nucleus becomes slightly more elongated. The fission time increases with the increase of dissipation and its distribution width becomes much wider, and the most probable fission time is proportional to the strength of the friction.

Based on the investigation of the effects of different friction formulas on mass distribution and TKE of fragments in 14 MeV $n + {}^{235}$U fission, we apply the friction formula W+W(a) to calculate the fission fragment mass distributions in 14 MeV $n + {}^{232-239}$U, ${}^{233-240}$Np, ${}^{235-242}$Pu, ${}^{237-244}$Am fission, and with this model most of the results agree well with the evaluated data and the GEF calculations, which verify the predictive power of this model. The systematic dependence of the averaged TKE on the Coulomb parameter is described as well, and it is overall consistent with the results of the systematic proposed by Itkis in 1998.

However, there are small deviations from the evaluated data and GEF predictions for mass distribution and TKE in some fissioning systems which implies further improvement is needed in both aspects of enlarging the dimensionality of Langevin equation and making more proper shell corrections in potential energy calculations.

ACKNOWLEDGMENTS

This work was supported by the National Natural Science Foundation of China under Grants No. 12105369, 11790324, 11790320, and by the Continuous Basic Scientific Research Project (No. WDJC-2019-09).

[1] P. Fröbrich, I. I. Gontchar, and N. D. Mavlitov, Nucl. Phys. A **556**, 281 (1993).
[2] Y. Abe, S. Ayik, P.-G. Reinhard, and E. Suraud, Phys. Rep. **275**, 49 (1996).
[3] P. Fröbrich and I. I. Gontchar, Phys. Rep. **292**, 131 (1998).
[4] T. Wada, Y. Abe, and N. Carjan, Phys. Rev. Lett. **70**, 3538 (1993).
[5] J. Bao, Y. Zhuo, and X. Wu, Z. Phys. A **352**, 321 (1995).
[6] T. Asano, T. Wada, M. Ohta, S. Yamaji, and H. Nakahara, J. Nucl. Radiochem. Sci. **7**, 7 (2006).
[7] Y. Aritomo and S. Chiba, Phys. Rev. C **88**, 044614 (2013).
[8] K. Mazurek, C. Schmitt, and P. N. Nadtochy, Phys. Rev. C **91**, 041603(R) (2015).
[9] M. R. Pahlavani and S. M. Mirfathi, Phys. Rev. C **93**, 044617 (2016)
[10] M. D. Usang, F. A. Ivanyuk, C. Ishizuka, and S. Chiba, Phys. Rev. C **94**, 044602 (2016).
[11] A. J. Sierk, Phys. Rev. C **96**, 034603 (2017).
[12] C. Ishizuka, M. D. Usang, F. A. Ivanyuk, J. A. Maruhn, K. Nishio, and S. Chiba, Phys. Rev. C **96**, 064616 (2017).
[13] H. Eslamizadeh and H. Raanaei, Phys. Lett. B **783**, 163 (2018).
[14] L. L. Liu, X. Z. Wu, Y. J. Chen, C. W. Shen, Z. X. Li, and Z. G. Ge, Phys. Rev. C **99**, 044614 (2019).
[15] A. V. Karpov, P. N. Nadtochy, D. V. Vanin, and G. D. Adeev, Phys. Rev. C **63**, 054610 (2001).
[16] C. Shen, G. Kosenko, and Y. Abe, Phys. Rev. C **66**, 061602(R) (2002).

[17] G. D. Adeev, A. V. Karpov, P. N. Nadtochii, and D. V. Vanin, Phys. Part. Nucl. **36**, 378 (2005).
[18] P. N. Nadtochy, E. G. Ryabov, A. E. Gegechkori, Yu. A. Anischenko, and G. D. Adeev, Phys. Rev. C **85**, 064619 (2012).
[19] P. Möller, D. G. Madland, A. J. Sierk, and A. Iwamoto, Nature (London) **409**, 785 (2001).
[20] K. Pomorski and J. Dudek, Phys. Rev. C **67**, 044316 (2003).
[21] C. Schmitt, K. Pomorski, B. Nerlo-Pomorska, and J. Bartel, Phys. Rev. C **95**, 034612 (2017).
[22] Z. Wang, W. Zhu, C. Zhong, and T. Fan, Nucl. Phys. A **989**, 81 (2019).
[23] Blocki, Y. Boneh, J. R. Nix, J. Randrup, M. Robel, A. J. Sierk, and W. J. Swiatecki, Ann. Phys. (NY) **113**, 330 (1978).
[24] K. T. R. Davies, A. J. Sierk, and J. R. Nix, Phys. Rev. C **13**, 2385 (1976).
[25] J. Randrup and W. J. Swiatecki, Nucl. Phys. A **429**, 105 (1984).
[26] H. Feldmeier, Rep. Prog. Phys. **50**, 915 (1987).
[27] S. Yamaji, H. Hofmann, and R. Samhammer, Nucl. Phys. A **475**, 487 (1987).
[28] H. Hofmann, Phys. Rep. **284**, 137 (1997).
[29] H. A. Kramers, Physica **7**, 284 (1940).
[30] A. J. Sierk and J. R. Nix, Phys. Rev. C **21**, 982 (1980).
[31] P. N. Nadtochy *et al.*, Phys. Lett. B **685**, 258 (2010).
[32] C. Schmitt, K.-H. Schmidt, A. Kelíc, A. Heinz, B. Jurado, and P. N. Nadtochy, Phys. Rev. C **81**, 064602 (2010).
[33] J. Sadhukhan and S. Pal, Phys. Rev. C **81**, 031602(R) (2010).
[34] J. Randrup, P. Möller, and A. J. Sierk, Phys. Rev. C **84**, 034613 (2011).
[35] D. Naderi, Phys. Rev. C **86**, 044609 (2012).
[36] H. Eslamizadeh, Int. J. Mod. Phys. E **21**, 1250008 (2012).
[37] N. Wang and W. Ye, Phys. Rev. C **97**, 014603 (2018).
[38] M. Mirea, L. Tassangot, C. Stephan, and C. O. Bacri, Nucl. Phys. A **735**, 21 (2004).
[39] A. Bulgac, S. Jin, K. J. Roche, N. Schunck, and I. Stetcu, Phys. Rev. C **100**, 034615 (2019).
[40] L. L. Liu, Y. J. Chen, X. Z. Wu, Z. X. Li, Z. G. Ge, and K. Pomorski, Phys. Rev. C **103**, 044601 (2021).
[41] P. V. Kostryukov, A. Dobrowolski, B. Nerlo-Pomorska, M. Warda, Z. Xiao, Y. Chen, L. Liu, J.-L. Tian, and K. Pomorski, Chin. Phys. C **45**, 124108 (2021).
[42] H. Hofmann, C. Grégoire, R. Lucas, and C. Ngô, Z. Phys. A **293**, 229 (1979).
[43] M. D. Usang, F. A. Ivanyuk, C. Ishizuka, and S. Chiba, Phys. Rev. C **96**, 064617 (2017).
[44] J. A. Maruhn and W. Greiner, Z. Phys. **251**, 431 (1972).
[45] A. V. Karpov and V. V. Saiko, Phys. Rev. C **96**, 024618 (2017).
[46] H. J. Krappe, J. R. Nix, and A. J. Sierk, Phys. Rev. C **20**, 992 (1979).
[47] A. J. Sierk, Phys. Rev. C **33**, 2039 (1986).
[48] M. Strutinsky, Nucl. Phys. A **95**, 420 (1967).
[49] M. Brack, J. Damgaard, A. S. Jensen, H. C. Pauli, V. M. Strutinsky, and C. Y. Wong, Rev. Mod. Phys. **44**, 320 (1972).
[50] A. V. Ignatyuk, K. K. Istekov, and G. N. Smirenkin, Sov. J. Nucl. Phys. **29**, 450 (1979).
[51] A. V. Ignatyuk, K. K. Istekov, and G. N. Smirenkin, Sov. J. Nucl. Phys. **21**, 255 (1975).
[52] J. Randrup and P. Möller, Phys. Rev. C **88**, 064606 (2013).
[53] W. J. Swiatecki, Nucl. Phys. A **428**, 199 (1984).
[54] J. R. Nix and A. J. Sierk, Nucl. Phys. A **428**, 161 (1984).
[55] D. A. Brown *et al.*, Nucl. Data Sheets **148**, 1 (2018).
[56] P. P. Dyachenko and B. D. Kuzminov, Sov. J. Nucl. Phys. **7**, 27 (1968).
[57] P. P. Dyachenko, B. D. Kuzminov, and M. Z. Tarasko, Sov. J. Nucl. Phys. **8**, 165 (1969).
[58] B. D. Wilkins, E. P. Steinberg, and R. R. Chasman, Phys. Rev. C **14**, 1832 (1976).
[59] H. Paşca, A. V. Andreev, G. G. Adamian, and N. V. Antonenko, Phys. Lett. B **760**, 800 (2016).
[60] H. Paşca, A. V. Andreev, G. G. Adamian, and N. V. Antonenko, Phys. Rev. C **104**, 014604 (2021).
[61] J.-F. Lemaître, S. Goriely, S. Hilaire, and J.-L. Sida, Phys. Rev. C **99**, 034612 (2019).
[62] K.-H. Schmidt, B. Jurado, C. Amouroux, and C. Schmitt, Nucl. Data Sheets **131**, 107 (2016).
[63] V. E. Viola, K. Kwiatkowski, and M. Walker, Phys. Rev. C **31**, 1550 (1985).
[64] M. G. Itkis and A. Ya. Rusanov, Fiz. Elem. Chastits At. Yadra **29**, 389 (1998) M. G. Itkis and A. Ya. Rusanov, [Phys. Part. Nucl. **29**, 160 (1998)].